Bioconjugate Chemistry

Article

pubs.acs.org/bc

Silica Nanoparticles and Polyethyleneimine (PEI)-Mediated Functionalization: A New Method of PEI Covalent Attachment for siRNA Delivery Applications

Yekaterina Kapilov Buchman,[†,§] Emmanuel Lellouche,[‡,§] Sally Zigdon,[‡,§] Moshe Bechor,[‡,§] Shulamit Michaeli,*[,‡,§] and Jean-Paul Lellouche*[,†,§]

[†]Department of Chemistry, Faculty of Exact Sciences, [‡]The Mina and Everard Goodman Faculty of Life Sciences, and [§]Institute of Nanotechnology and Advanced Materials, Bar-Ilan University, Ramat-Gan, 5290002 Israel

Supporting Information

ABSTRACT: Small-interfering RNA (siRNA) is a synthetic double-stranded RNA that consists of approximately 21 nucleotides (nts). It induces degradation of target mRNAs in a sequence-specific manner by the RNA interference (RNAi) mechanism. Thus, siRNAs offer a potential strategy for silencing mutated or defective genes that cause a variety of human diseases. The main obstacles of harnessing siRNAs as drugs are their inefficient delivery to cells and off-target effect making clinical applications very challenging. To address these issues, researchers have studied a variety of nanocarrier systems for siRNA delivery. This study presents the design, fabrication, and full characterization of innovative polyethyleneimine (PEI)-decorated polycationic 34.2 ± 4.2 nm silica (SiO_2) NPs for siRNA-mediated gene silencing. More specifically, a new means of introduction (covalent mode of attachment) of the polycationic 25 kDa PEI polymer onto the SiO_2 NP surface has been developed that makes use of an effective electrophilic double Michäel acceptor, divinyl sulfone (DVS). The resulting novel SiO_2−PEI nanoparticles (SPEI NPs) have been fully characterized using a wide range of analytical, spectroscopic, and microscopic methods (TEM, DLS, ζ potential, elemental analysis (EA), XPS, TGA, and FTIR). Disclosing quite low cytotoxicity due to this unique mode of PEI covalent grafting, SPEI NPs/siRNA polyplexes have been successfully tested for the induction of gene silencing using dual-reporter luciferase transfected human osteosarcoma U2OS cells. The corresponding gene silencing data showed a clear correlation between PEI/siRNA ratios, siRNA concentration(s), and the level of gene silencing. Moreover, these SPEI NPs have been demonstrated to be thermodynamically stable with an ability to efficiently bind siRNAs and induce silencing for at least a one-year-long storage.

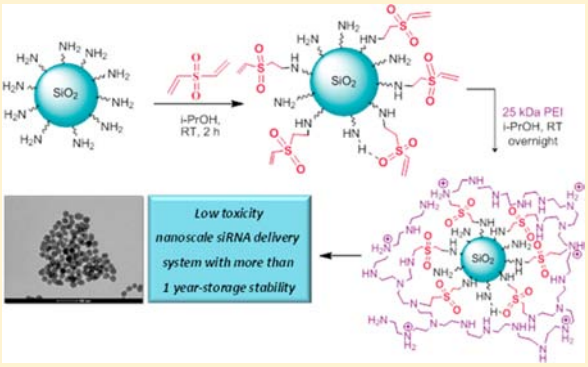

INTRODUCTION

RNA interference (RNAi) using small interfering RNA (siRNA), a 19−21 base pair double-stranded RNA, has been considered as a potential therapeutic breakthrough for the treatment of variety of diseases such as cancer and infectious diseases.[1,2] Naked siRNAs are subject to degradation by endogenous enzymes. In addition, such large molecules (≈16 kDa) are strongly negatively charged, being unable to cross cellular membranes. In this context, the safe, effective, and targeted intracellular delivery of siRNA species represents a highly challenging barrier for making siRNA technology suitable for clinical utilization. To date, a number of advanced materials, including neutral and/or cationic polymers,[3−5] cell-penetrating peptides,[6,7] amphoteric lipid-based carriers,[8,9] cyclodextrins,[10,11] dendrimer platforms,[12,13] as well as various nanoparticle formulations,[14−18] have been investigated for their potential as siRNA delivery agents. The resulting nano-constructs have been shown to possess the attractive capabilities of cell penetration and siRNA cargo release in the cytoplasm, where the RNAi machinery is initiated.

One of the most well-characterized and efficient transfecting agents for siRNA is a group of branched or linear polyethylenimine polymers (PEIs) that possess high positive charge density due to the presence of ammonium (NH_4^+) ions. PEI polymers have been widely used as coating material for inorganic nanoparticles (NPs) as well as polymeric carriers for gene delivery because of their strong electrostatic affinity for polynucleic acids. They also disclose a key efficient endosomal escape capability via the "proton sponge" effect after intracellular uptake. However, the known nonspecific cytotoxicity of high molecular weight PEIs caused by the destabilization of cellular and mitochondrial membranes and by the activation of intracellular apoptotic signals strongly limits the clinical

Received: September 24, 2013
Revised: October 27, 2013
Published: November 4, 2013

   dx.doi.org/10.1021/bc4004316 | *Bioconjugate Chem.* 2013, 24, 2076−2087

application of this polymer.[19−21] Various chemical modifications by small molecules, neutral biocompatible polymers, and cross-linking have recently been proposed and vigorously investigated to reduce this strongly limiting nonspecific cytotoxicity while maintaining superior polynucleic acid delivery effectiveness and endosome escape.[22−27]

Among the various integrated organic and inorganic nanocomposite systems described in the field, inorganic silica (SiO_2)-based nanostructured particles have attracted great interest due to their ease of formation, low cytotoxicity, excellent chemical stability, and great versatility for potential surface modifications. A wide range of clinical applications is thus possibly applicable for SiO_2 NPs, including theranostics (combined diagnosis and therapy features), drug delivery, gene transfection, and multimodal imaging.[28−32] Indeed, a few works described the fabrication and use of PEI-functionalized SiO_2 NPs as nanovectors for *in vitro* siRNA delivery. For example, Xia et al.[33] used various branched PEIs of different molecular weights (0.6−25 kDa range) that were electrostatically noncovalently attached onto 100−130-nm-sized negatively charged mesoporous SiO_2 NPs (MSNPs), accounting for approximately 5% of any construct weight. The corresponding MSNP-PEI constructs formed complexes with siRNA molecules. Thus, silencing of green fluorescent protein (GFP) using 30 nM siRNA bound to polyplexes prepared from 10 and 25 kDa PEI polymers resulted in mRNA reduction by a 55% and 60% factor, respectively. In another study, Li and co-workers[34] successfully loaded siRNA into mesopores of magnetic mesoporous SiO_2 NPs with a particle size of ≈50 nm under strongly dehydrated conditions, followed by noncovalent coating with 25 kDa PEI polymer. The resulting constructs were able to down-regulate the endogenous Bcl-2 gene using 50 nM siRNA for an almost 80% level of silencing.

In this study, we used amorphous 32.8 nm SiO_2 NPs as a versatile nanoscale nanoparticulate platform for siRNA delivery into stable expressing dual-reporter U2OS cells (osteosarcoma mammalian cells). The corresponding surface engineering of such core SiO_2 NPs has been designed using an innovative and effective covalent coupling method. Indeed, the outer shell of this siRNA delivery system was composed of a thin layer of a branched 25 kDa PEI polymer covalently attached onto intermediate poly-NH_2-functionalized SiO_2 NPs using the highly reactive *bis*-Michäel acceptor divinyl sulfone (DVS, $(CH_2{=}CH)_2SO_2$). DVS can readily react with nucleophilic groups such as -NH_2, -SH, and -OH (alcohol) in basic conditions[35−37] and was already successfully used as a linker in former works.[38,39] Here and for the first time, we provide strong evidence that DVS chemistry (double Michäel electrophilic addition) can be successfully exploited to link a bulky 25 kDa PEI polymer onto the poly-NH_2 SiO_2 NP surface to produce NPs harboring stable and effective silencing capabilities. A relatively high molecular weight 25 kDa PEI polymer was chosen for SiO_2 NPs grafting for its well-known superior ability to effectively compact and deliver siRNA. Beyond the basic reactive grafting capability of DVS for PEI attachment, this grafting method also operates via selective primary amine (PEI, R-NH_2) chemical modifications of the PEI polymeric phase.[36] As a matter of consequence and as demonstrated in this study, the well-known well-documented high toxicity of the 25 kDa branched PEI polymer within SPEI NPs might be seriously mitigated due to this specific DVS linker chemical manipulation that mainly acts on the primary NH_2 groups of PEI. To the best of our knowledge, this is the first time that such a bifunctional linker that enabled PEI covalent grafting onto SiO_2 NPs has been used to simultaneously reduce its intrinsic cellular toxicity. Consequently, such a DVS-mediated chemical manipulation of resulting SPEI NPs (shell engineering) strongly suggested that this new PEI grafting methodology might be considered as a useful alternative to the use of similar gene silencing effective PEI polymers of much lower molecular weights.

Various characterization methods, such as transmission electron microscopy (TEM), dynamic light scattering (DLS), surface ζ potential, X-ray photoelectron spectroscopy (XPS), elemental and thermogravimetric (TGA) analyses, in addition to FTIR spectroscopy and primary amine (NH_2) quantification (UV-sensitive Kaiser test), have been used to investigate and characterize the different morphological and functional properties of the corresponding intermediate and final functional nanostructures. Moreover, we show that SPEI NPs form reasonably stable polyplex dispersions with siRNAs in DMEM (a serum containing biological medium) with hydrodynamic sizes (DLS) not much altered from those measured in H_2O, demonstrating their good solubility without any tendency for uncontrolled aggregation. For the first time, such NPs were tested for long-range thermodynamic stability. Moreover, all silencing assays were based on the dual-luciferase system, which simultaneously provides highly precise quantitative silencing data, with internal control for cytotoxic effects of the functional nanomaterial.

MATERIALS AND METHODS

Materials. Tetraethyl orthosilicate (TEOS, 99.999%), ammonium hydroxide (ACS reagent, 28−30%), divinyl sulfone (DVS, 97%), polyethyleneimine (PEI-25, branched, MW ≈25,000 Da), fluorescein isothiocyanate (FITC ≥ 90% HPLC), phenol (ACS, ≥ 99.5%), and ninhydrin (ACS reagent) were purchased from Sigma-Aldrich (Israel). (3-Aminopropyl)-triethoxysilane (APTS, 99%) was purchased from Acros Organics.

Dulbecco's modified Eagle's medium (DMEM), penicillin−streptomycin amphotericin B solution, and L-glutamine solution (29.2 mg/mL in saline -200 mmol/liter) were purchased from Biological Industries (Israel). A double stranded siRNA for Luciferase knockdown with 2 nucleotides 3′ overhangs in antisense strand (5′-UGUAAAAGCAAUUGUUCCAGGAAC-CAG-3′; molecular weight of duplex 16,553) was purchased from IDT Technologies (Coralville, IA). The Dual-Glo Luciferase Assay System was from Promega (Madison, WI, USA). LysoTracker Red DND-99 was purchased from Invitrogen (Carlsbad, CA, USA). All experiments and analyses used deionized water. All chemicals and solvents were reagent grade and were used without any further purification or modification.

PEI-Functionalized SiO_2 Nanoparticle (SPEI NP) Synthesis. SiO_2 NPs were synthesized by a general method that includes hydrolysis and further condensation of the silicate source in ethanol under basic conditions. The exact procedure included dissolution of ammonium hydroxide (2.4 mL, ≈18 mmol) in absolute ethanol (60 mL) followed by addition of TEOS (2.4 mL, 10.7 mmol). In the case of fluorescent NPs, FITC-APTS conjugate solution (150 μL, ≈2 μmol) was added next, and the vessel was wrapped with aluminum foil to protect FITC from bleaching. The reaction was stirred overnight at ambient temperature until formation of NPs was complete. Then, EtOH (40 mL) was added, as well as APTS (500 μL,

dx.doi.org/10.1021/bc4004316 | Bioconjugate Chem. 2013, 24, 2076−2087

2.137 mmol); the reaction was then stirred for another 24 h. The resulting poly-NH_2-SiO_2 NPs (SPA NPs) were cleaned to remove excess ammonium hydroxide and other compounds by repeated centrifugation−sonication−redispersion in a water−ethanol mixture for three cycles, followed by the same action with absolute EtOH.

To synthesize fluorescent SiO_2 NPs, the fluorescent compound FITC was first conjugated with (3-aminopropyl)-triethoxysilane (APTS) to yield a silyl-reactive compound. The general procedure included dissolution of FITC (5.25 mg, 0.0135 mmol) in dry THF (1 mL) followed by addition of APTS (67 μL, 0.286 mmol) and stirring at ambient temperature overnight. The conjugate was used as fresh solution without further purification.

To further functionalize nanoparticles, DVS (28 μL, 0.28 mmol) was added into a sonicated dispersion of SPA NPs in *i*-PrOH (350 mg in 80 mL, 0.21 mmol of $-NH_2$). The amount of DVS taken was equivalent to the number of moles of primary amines on the surface of SPA NPs. The reaction was stirred for 2 h at ambient temperature, followed by one cycle of washing and redispersion in *i*-PrOH. To the freshly prepared and sonicated (5 min) NPs (280 mg in 60 mL), 25 kDa PEI solution (280 mg in 2 mL *i*-PrOH) was added, and the reaction was sonicated for 5 min and then allowed to stir overnight. After the reaction was completed, the excess PEI was washed by three cycles of centrifugation, and the modified SiO_2−PEI NPs (SPEI NPs) were redispersed in EtOH.

PEI-Noncovalently Bound SiO_2 (SiO_2@PEI) NP Synthesis. A 25 kDa PEI H_2O solution (6 mg, 1 mL) was added into a H_2O suspension of SPA NPs (30 mg, 5 mL) and stirred overnight. At completion, the excess of PEI was washed by three cycles of centrifugation, and the SiO_2@PEI NPs were redispersed in H_2O.

Physicochemical Characterization. The following properties of SiO_2 NPs were characterized: size, shape, size distribution, surface charge, elemental analysis, surface atomic composition (XPS), FTIR spectrum, and amount of organic matter (TGA).

Transmission Electron Microscopy. The size, shape, and size distribution of nanoparticles were measured using a transmission electron microscope (FEI Tecnai Spirit Bio-Twin, Oregon, USA) that was equipped with a Gatan MS 794 CCD camera. Samples for TEM imaging were prepared by placing a drop of diluted EtOH dispersion (200−250 μg/mL) onto a 400-mesh copper TEM grid (400C-FC, Electron Microscopy Sciences, Hatfield, PA, USA) and then drying at ambient temperature for 1−2 h. A minimum of five images of each sample was collected to obtain representative values. Mean diameter size and size distribution were collected by measuring the diameter of at least 170 NPs using ImageJ software, an image processing program developed at the National Institutes of Health. The major diameter was taken into account when the NP had ellipsoidal geometry.

DLS and ζ Potential. The size and surface charge of NPs in dispersion were measured by a ZetaSizer Nano-ZS (Malvern Instruments Ltd., Worcestershire, UK). Size measurements were performed by the dynamic light scattering (DLS) method of dilute nanoparticle dispersions (≈0.5 mg/mL) in EtOH, *i*-PrOH, or H_2O. The samples were sonicated for 1−2 min before analysis. The ZetaSizer Nano series was also used for determining the ζ potential of NPs by measuring electrophoretic mobility and then applying the Henry equation.

Elemental Analysis. The total nitrogen, carbon, and sulfur contents of all silica NPs were analyzed using the CHNS Analyzer Model FLASH EA 1112 series made by Thermo Finnigan, Italy. During analysis, combustion of a sample occurs at 1000 °C to produce gases of H_2O, CO_2, N_2, SO_3, and SO_2. The mixture of the gases was separated by a GC column, and quantitative analysis was performed by the detection of signals. The results are represented by weight percentage of each element.

Ninhydrin Quantitative Test for Primary Amines. The Kaiser Test was used for primary amine quantification (for the detailed procedure, see Supporting Information).[40]

X-ray Photoelectron Spectroscopy. XPS analysis was carried out using a Kratos Axis HS apparatus equipped with an ultrahigh vacuum chamber (5×10^{-10} Torr) containing samples loaded onto a double-sided carbon-based self-adhesive tape (complete coverage).

Thermogravimetric Analysis (TGA) and Differential Scanning Calorimetry (DSC). TGA and DSC analyses were performed simultaneously by a TGA/DSC1 analyzer (Mettler-Toledo, OH, USA) for which dry NPs (8−10 mg) were taken. Thermograms were recorded in air at a heating rate of 20 °C min^{-1} over the temperature range 25−800 °C. Weight change and heat flow were measured simultaneously during the analysis.

FTIR. FTIR spectra were recorded on a Bruker TENSOR 27 spectrometer using a Diffuse Reflectance Accessory EasyDiff (PIKE Technologies). Samples were prepared by mixing SiO_2 powder with IR grade KBr. The spectra obtained by the diffuse reflection technique appear different from standard transmission spectra. The peak intensities at high wavenumbers are weak, and the peak-line shapes are rounded. To compensate for these differences, the spectra were transformed into Kubelka−Munk units using FTIR software.

Preparation of SPEI NPs/siRNA Complexes and Determination of Binding Ability Using NanoDrop Technology. To determine the amount of siRNA adsorbed on the SPEI NP surface, a series of dispersions was prepared. The addition of a constant amount of siRNA solution (5 μg) into H_2O dispersions of SPEI NPs with different NP concentrations (0.51, 1.02, 2.05, 3.07, 4.1, and 8.2 mg/mL) gave a series of various PEI/siRNA w/w ratios (0.14, 0.28, 0.56, 0.84, 1.12, and 2.24). A sample with the same siRNA concentration but without NPs was used as the control. The final volume of each sample was 24.4 μL. The polyplexes were allowed to form (15 min, ambient temperature) and precipitated by centrifugation (13,500 rpm, 4 °C, 12 min). The concentration of siRNA in the residue liquid was determined by means of light absorption in the UV range, performed by NanoDrop, a spectrophotometer for microrange volumes (Thermo Scientific, Wilmington, USA). Only the unbound siRNA gave a UV signal that was comparable to the siRNA concentration in the control sample. The amount of bound siRNA was easily calculated by dividing the difference between control and sample absorption by the control absorption value that represented 100% free siRNA.

Preparation of SPEI NPs/siRNA Polyplexes for DLS and ζ Potential Measurements. To obtain the size and ζ potential of SPEI NPs/siRNA polyplexes with different weight ratios, a series of dispersions was prepared in the following manner. The addition of varied amounts of siRNA (11.2, 5.6, 2.2, 1.1, 0.7, and 0.6 μg) into a constant amount of SPEI NPs (200 μg, 100 μL) gave a series of various PEI/siRNA w/w

Scheme 1. Fabrication of SiO_2-PEI NPs (SPEI NPs) via Coupling with DVS as a Linker

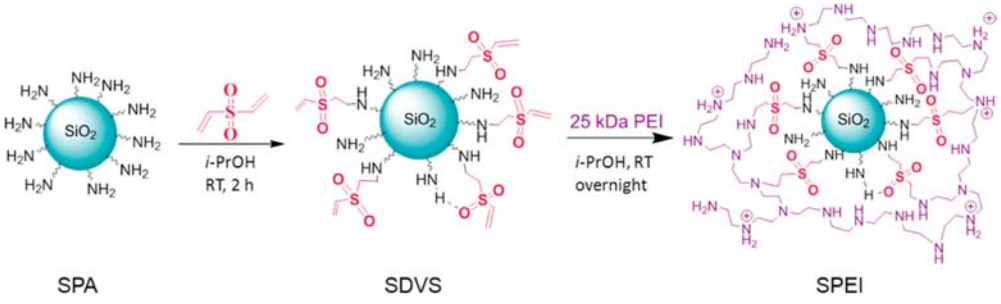

ratios (1, 2, 5, 10, 15, and 20). The polyplexes were allowed to form (15 min, ambient temperature), and H_2O (900 μL) was added to each sample to create sufficient volume for analysis. A sample without siRNA was also prepared by the same manner. Size and ζ potential were measured for each sample in triplicate repetition mode.

Investigation of the Polyplex Behavior in DMEM. To obtain the sizes of SPEI NPs/siRNA polyplexes with different weight ratios, a series of dispersions was prepared in the following manner. The addition of varied amounts of siRNA (6.7, 3.4, 1.3, and 0.7 μg) into a constant amount of SPEI NPs (120 μg, 60 μL) gave a series of PEI/siRNA w/w ratios (1, 2, 5, and 10). The polyplexes were allowed to form (15 min, ambient temperature), and DMEM (540 μL) was added into each sample. A sample without siRNA was also prepared by adding DMEM to SPEI NPs in the same manner. After DLS measurement (triplicate), a sample was held in an ultrasonic bath (1 min), and size measurement was repeated in triplicate repetition mode.

Chemical Stability of SPEI NPs. An H_2O dispersion of SPEI NPs (1 μg/μL) with seven weeks exposure at 4 °C was centrifuged, and the supernatant (80 μL) was collected for Kaiser Test analysis. The amount of primary amines in this sample was compared to that in a 25 kDa PEI H_2O solution of known concentration (0.1 mg/mL, 80 μL). An additional sample was prepared by collecting a supernatant (100 μL) from an EtOH dispersion of SPEI NPs (4.9 μg/μL) with five months exposure at 4 °C. The control sample for this experiment was a 25 kDa PEI EtOH solution (0.1 mg/mL, 100 μL). Kaiser Test was performed over the samples as described in the Supporting Information with no final dilution (factor 10). Each sample was tested with triplicate repetition. From the known values of control samples, the unknown PEI concentrations were calculated using the rule of three. The maximum theoretical amount of PEI in H_2O samples is 4.4 μg (1 μg/μL × 80 μL × 0.055 μg of PEI/μg of NPs), and in EtOH samples, 27.0 μg (4.9 μg/μL × 100 μL × 0.055 μg of PEI/μg of NPs). The percentage of detached PEI was calculated using the theoretical value and observed PEI concentration.

Confocal Microscopy of Cellular Uptake of SPEI/siRNA Polyplexes. To perform intracellular trafficking, NPs were labeled with fluorescein isothiocyanate (FITC) according to the procedure mentioned in the experimental section above.

Transfected U2OS cells were seeded onto 18 mm coverslip glass in 12-well plates at a density of 5 × 10^4 cells/well containing 1 mL complete medium and were incubated for 24 h at 37 °C in humidified 5% CO_2 atmosphere for adherence. SPEI NPs (25 μg) were mixed with siRNA (0.63 μg) for 15 min prior to addition into the cells for incubation. After 24 h, LysoTracker was added to samples for 1 h. Then, samples were washed four times with phosphate-buffered saline (PBS, 1 mL), stabilized with 4% paraformaldehyde (0.5 mL) for 20 min, and washed again with PBS. Nuclei were stained with 4′,6-diamidino-2-phenylindole (DAPI) for 10 min and were washed with PBS. Immu-Mount was used to resist fading. Images were taken using a confocal Laser Scanning Microscope, (CLSM), Leica TCS SPE (×63), and then the 3D images were edited in the software Imaris, Bitplane.

***In Vitro* siRNA Transfection with SPEI NPs/siRNA Polyplexes.** *Optimal PEI/siRNA Mass Ratio Determination.* Human osteosarcoma U2OS cells were cultured in a Dulbecco's modified Eagle medium (DMEM) containing 10% fetal calf serum (FCS), 1% antibiotic cocktail of streptomycin + penicillin, and 1% L-glutamine and maintained at 37 °C in a humidified 5% CO_2 atmosphere. To perform siRNA experiments, U2OS cells were prior transfected with plasmid psiCHECK-2 Vector that contained *Renilla* luciferase, which is used as the primary reporter gene, and *Firefly* luciferase, the second reporter gene. Transfected U2OS cells were seeded into 96-well plates at a density of 5 × 10^3 cells/well containing 100 μL complete medium and were incubated for 24 h for adherence. SPEI NPs/siRNA polyplexes were prepared by addition of a constant amount (0.166 μg, 0.01 nmol) of *Firefly* luciferase specific siRNA into various amounts of SPEI NP (2.96 5.93, 14.82, 29.64, 44.46, and 59.29 μg) suspensions obtaining different PEI/siRNA w/w ratios (1, 2, 5, 10, 15, 20). The formation of polyplexes was assured by incubation of the mixtures for 15 min at ambient temperature. The resulting SPEI NPs/siRNA suspensions were added into the cells, and gene expression levels were recorded 48 h after transfection without any medium change. Each NP/siRNA ratio was added in triplicate mode, and each experiment was repeated three times.

Optimal siRNA Concentration Determination. A series of SPEI NPs/siRNA polyplexes was prepared by addition of different amounts (16.6 (1.0), 33.2 (2.0), 66.4 (4.0), 99.6 (6.0), 132.8 (8.0) and 166.0 (10.0) ng (pmol)) of *Firefly* luciferase specific siRNA into various amounts of SPEI NP (1.48, 2.96, 5.93, 8.89, 11.86, and 14.82 μg) suspensions, maintaining a constant PEI/siRNA w/w ratio of 5. The formation of polyplexes was secured by incubation of the mixtures for 15 min at room temperature. The resulting SPEI NPs/siRNA suspensions were added into the cells, and gene expression levels were recorded 48 h after transfection without any medium change. Each NP/siRNA ratio was added in triplicate mode, and each experiment was repeated three times.

Gene Silencing Analysis. Quantitative analysis of gene silencing efficacy was carried out using a Dual-Luciferase Reporter 1000 Assay System. After 48 h of transfection, cells were washed with PBS and lysed by incubating with 1 × PLB

dx.doi.org/10.1021/bc4004316 | *Bioconjugate Chem.* 2013, 24, 2076−2087

(Passive Lysis Buffer) (20 μL) for 25 min. Luciferase Assay Reagent II was then injected (100 μL) into each well, and *Firefly* luciferase activity was quantified by measuring the photon luminescence emission at 560 nm using a Sinergy 4 Spectrophotometer Elisa plate reader. Then Stop & Glo Reagent was injected (100 μL) into each well; this reagent simultaneously quenches *Firefly* luciferase activity and activates luminescence from *Renilla* luciferase, which was measured at 510 nm.

RESULTS

Synthesis and Decoration of SiO_2 Nanoparticles for siRNA Delivery/Gene Silencing. Branched PEI-decorated SiO_2 nanoparticles were prepared by three sequential simple synthetic steps (Scheme 1). First, SiO_2 NPs were formed using a classical Stöber method that includes hydrolysis and subsequent condensation of TEOS ($Si(OEt)_4$) in basic conditions. After mixing TEOS and a 28% w/w NH_4OH aqueous solution in EtOH at ambient temperature, 32.8 nm NPs were formed. Furthermore, poly-NH_2 functionalization of the resulting SiO_2 NPs occurred without any purification steps by addition of APTS ($(EtO)_3Si\text{-}(CH_2)_3NH_2$), which binds to the SiO_2 NP surface through hydrolysis of ethoxysilane groups and results in the formation of poly-NH_2-SiO_2 NPs (SPA NPs). For further PEI polymer attachment, DVS was used as a linker for covalent grafting of the PEI phase onto the SPA NP surface (Scheme 1). DVS is a homobifunctional molecule that is characterized by its high electrophilic reactivity, undergoing rapid Michäel additions with nucleophilic -NH_2 groups. Thus, the second synthetic step included the linkage of one tail-end of DVS with primary amines (poly-NH_2 shell) on the SiO_2 NP surface without base catalysis, resulting in the formation of SiO_2-DVS NPs (SDVS NPs). In the third step, addition of branched 25 kDa PEI to SDVS NPs readily afforded PEI-functionalized SiO_2 NPs (SPEI NPs). After SDVS NP precipitation (a rapid centrifugation step) and subsequent redispersion in *i*-PrOH, the second slower Michäel addition reaction [41] that mainly occurs between PEI primary amines and available second vinyl sulfone species was performed. Secondary amines have very low reactivity toward activated vinyl groups.[36] *i*-PrOH was chosen as the optimal Michäel addition chemistry-based reaction solvent because it is (i) a convenient dispersant for SiO_2 NPs and (ii) an appropriate solvent for PEI, which, along with its quite low reactivity toward DVS, thus strongly minimizes the potential for competitive side reactions via DVS neutralization.

Physicochemical Characterization of Intermediate and Functional NPs. Each synthetic step significantly changes the typical characteristics of the nanoparticle surface. Indeed, both NP hydrodynamic diameters (DLS Ø) and ζ potential values were monitored, and the corresponding alterations are consistent with the engineering surface chemistry described in Table 1. Indeed, bare SiO_2 NPs disclosed a negative ζ potential value, i.e., −26.5 mV, that is typical for SiO_2 NPs. They are rather aggregated when suspended in *i*-PrOH (DLS Ø: 630 nm, polydispersivity PDI: 1.0). Second, the relatively low positive ζ potential of SPA NPs (+20.6 mV) is explained by the surface charge shielding toward zero by the negative silanol Si-OH groups of the SiO_2 phase. This NP hydrodynamic size is approximately 4 times larger (140.8 nm) than the actual average nanoparticle one measured by TEM (32.8 nm, Figure 1A). They are much smaller than bare nontreated significantly aggregated SiO_2 NPs. This is likely due to an effective grafting

Table 1. Size (TEM, DLS) and ζ Potential (Electrophoretic Mobility) Characteristics of Intermediate and Final NPs in *i*-PrOH

NP type	TEM diameter [nm]	Z-average [nm]	Zeta potential [mV]
Bare SiO_2	31.5 ± 5.2	630 ± 74	−26.5 ± 0.3
SPA	32.8 ± 4.2	140.8 ± 3.9	+20.6 ± 2.0
SDVS	[a]	>10,000 nm - clusters	−3.8 ± 0.1
SPEI	34.2 ± 4.2	304.7 ± 4.9	+26.6 ± 1.0

[a]Nonrelevant data at this fabrication stage.

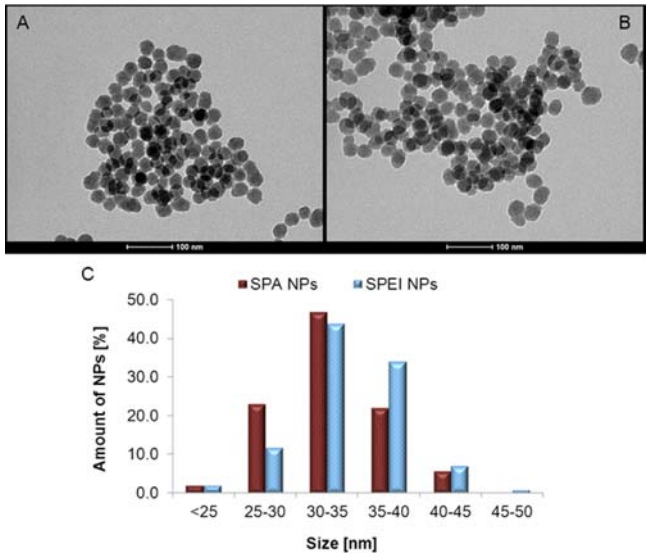

Figure 1. TEM images and size distribution of functional SiO_2 NPs: (A) SPA NPs, (B) SPEI NPs (scale bar of 100 nm), and (C) size distribution histograms.

of surface organic aminopropyl species. In the second step of surface modification using DVS, the resulting SDVS NPs disclosed a very small negative ζ potential value of −3.8 mV that resulted in a nonstable colloidal system, with the formation of micrometric, large aggregated clusters of NPs that formed due to increased surface tension energy. Interestingly, such generated clusters are most likely reversibly assembled, as they do not detrimentally affect the final PEI-related NP functionalization step. DVS-mediated PEI attachment onto the NP SiO_2 surface is characterized by a much lower aggregation level, with an average NP hydrodynamic size in the 304.7 nm range. PEI conjugation has also been confirmed by the measurement of an average increased positive surface charge close to +26.2 mV. In addition, the averaged TEM SPEI NP size (*ImageJ* software, at least 180 measured objects) revealed that the NP TEM size minimally changed by only 1.4 nm *before* and *after* PEI grafting, from 32.8 to 34.2 nm, respectively (Figure 1A-C).

To better explore and quantify NP surface modifications occurring during these grafting steps, both nanoparticulate elemental analysis (EA) and ninhydrin-based Kaiser Tests [40] for primary amine (R-NH_2) quantification have been performed (Table 2). The N elemental weight percentage increased from 0.96% to 3.05% when moving from SPA to SPEI NPs, confirming the presence of the grafted polyaminated 25 kDa PEI phase. Interestingly, the relative carbon amounts also increased from the initial SPA NPs (2.86%) to the intermediate SDVS NPs (4.16%) toward the final SPEI NPs (7.86%). This C

dx.doi.org/10.1021/bc4004316 | *Bioconjugate Chem.* 2013, 24, 2076−2087

Table 2. Elemental Analysis (EA, Values Given as Weight Percentage) and Kaiser Test Values of Surface-Modified SiO_2 NPs

NP type	Nitrogen	Carbon	Sulfur	Kaiser Test [mmol/g]
SPA	0.96	2.86	0.00	0.61
SDVS	0.92	4.16	0.59	0.30
SPEI	3.05	7.86	0.40	0.51

elemental feature evolution is quite consistent with a step-dependency of carbonaceous material grafting. Moreover, the S element was not detected before NP surface modification using DVS. After DVS grafting, the S weight percentage, 0.59%, decreased with the next PEI shell formation to 0.4% for SPEI NPs. Kaiser Test values for modified NPs also fully agreed with performed surface chemistries. Indeed, Kaiser Test values of 0.61 and 0.30 mmol accessible NH_2 groups/g NPs *before* and *after* DVS attachment, respectively, were obtained; the ratio of 0.49 implies that more than 50% of the primary amines reacted with the DVS linker. Similar Kaiser testing for final SPEI NPs exhibited a higher value (0.51 accessible NH_2 groups/g NPs) than for SDVS NPs but was slightly lower for the polyaminated SPA NPs.

NP surface elemental modifications can also be readily tracked using surface-sensitive X-ray photoelectron spectroscopy (XPS, Table 3). Thus, Si, C, N, and S atomic contents have

Table 3. XPS Analysis Data for Surface-Modified SiO_2 NPs (the Given Values Are Relative Atomic Concentration Percentages)

Entry	NP type	Silicon	Carbon	Nitrogen	Sulfur
1	SiO_2	58.39	41.6	0.01	0.00
2	SPA	40.31	53.83	5.86	0.00
3	SDVS	34.04	59.92	4.24	1.79
4	SPEI	19.68	70.63	8.84	0.84

been analyzed for (i) pure SiO_2 NPs (entry 1) that served as control and (ii) the three differently modified NPs (entries 2–4). Relative amounts of Si decreased from 58.39% to 19.68% when moving from pure SiO_2 NPs toward PEI-decorated ones via intermediate values of 40.31% and 34.04% (entries 2–3) for both SPA and SDVS NPs, respectively, due to the shielding effect of the outer PEI phase. C atomic concentrations regularly increased with each synthetic step from 41.6% (pure SiO_2 NPs) to 70.63% for final fully functional SPEI NPs. Moreover, tracking N atomic contents (values of 5.86% and 8.84% for SPA and SPEI NPs, respectively) also provides clear evidence of the N-enriched PEI decoration of the final SPEI NPs (entries 2 and 4). Its percentage was reduced after addition of DVS, confirming the shielding effect induced by the new layer. Interestingly, the S element was observed only after NP surface modification using DVS (entry 3). This same S element also disclosed a clear decrease in atomic content from 1.79% (entry 3) to 0.84% (entry 4) *before* and *after* the PEI grafting, which is fully consistent with the shielding effect of the outer PEI phase.

In this context, and for improved NP characterization, weight amounts of the PEI component in fully functional SPEI NPs have been quantified using thermogravimetric analysis (TGA). Weight loss tracking involved the former four types of untreated and chemically modified SiO_2 NPs (Figure 2). Such TGA analyses have been conducted in the temperature range of 25–800 °C (air flow with a 20 °C/min increasing temperature profile). Accordingly, each NP functionalization step showed overall increasing percentages of decomposable matter from 16.9% for untreated SiO_2 NPs to 27.23% for PEI-decorated SPEI ones (Table 4). The corresponding weight loss graphs show few-step profiles as defined by first derivative curves (DTG) for each NP material (Figure S3 and Table 4). Generally speaking, the first 25–200 °C NP weight losses corresponded to the evaporation of moisture and adsorbed low-weight solvents.[42] Additional observed weight loss steps indicated the behavioral complexity of decomposition of the various covalently attached organic phases. More specifically, pure untreated SiO_2 NPs disclosed one unique additional weight loss step (DTG minimum at 476 °C, Figure S3-A) that likely arose from the combustion of nonhydrolyzed silylethoxy (Si-OEt) groups present in the inorganic SiO_2 phase.[42] SPA NPs for which APTS has been conjugated to the SiO_2 NP surface exhibited two additional weight loss steps, with 330 and 500 °C DTG minima and weight losses of 9.33% and 5.28%, respectively (Figure S3–B), indicative of the presence of a polyamine shell.[43] Similar TGA weight losses and DTG profiling also arose from DVS modification, with minima at 311 and 513 °C related to 6.37% and 6.30% weight losses, respectively (Figure S3–C). PEI attachment on the DVS-activated surface of the corresponding SDVS NPs led to functional SPEI NPs that disclosed three clearly defined weight loss steps, with 210, 343, and 522 °C DTG minima that characterize 3.43%, 8.52%, and 6.21% weight loss percentages, respectively (Figure S3-D). This result is likely due to a more complex NP surface functionalization pattern arising from surface 2D vinylsulfone/NH_2-mediated PEI cross-linking. Comparison of this NP TGA profile with that of the pure 25 kDa PEI polymer featuring three-step weight losses (Figure 2 and Table 4) reveals that complete loss in the 25–790 °C temperature range enabled PEI phase quantification. Indeed,

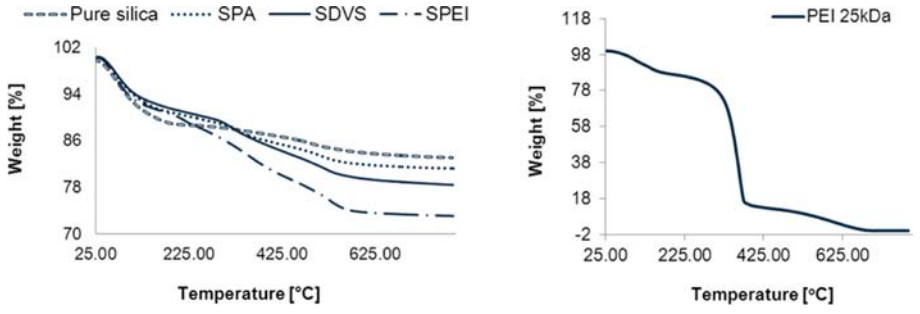

Figure 2. (*Left*) Weight loss curves (TGA) of (i) untreated SiO_2 and (ii) chemically modified SiO_2 NPs (three types); (*right*) TGA curve of pure 25 kDa PEI polymer.

dx.doi.org/10.1021/bc4004316 | *Bioconjugate Chem.* 2013, 24, 2076–2087

Table 4. Temperature-Dependent TGA Weight Loss Steps with Quantified Data

NP type	1st step Temp range [°C]	1st step Weight loss [%]	2nd step Temp range [°C]	2nd step Weight loss [%]	3rd step Temp range [°C]	3rd step Weight loss [%]	4th step Temp range [°C]	4th step Weight loss [%]	[a]Org. matt. [%]
Pure SiO_2	25–220	11.32	220–790	5.58					5.58
SPA	25–180	9.33	180–368	4.49	368–790	5.28			9.77
SDVS	25–208	9.28	208–410	6.37	410–790	6.30			12.67
SPEI	25–160	9.07	160–260	3.43	260–446	8.52	446–790	6.21	18.16
PEI polymer	25–205	13.35	205–450	74.46	450–790	12.11			86.57

[a]The last column reports weight loss values for the total organic matter, excluding losses of H_2O and volatile compounds.

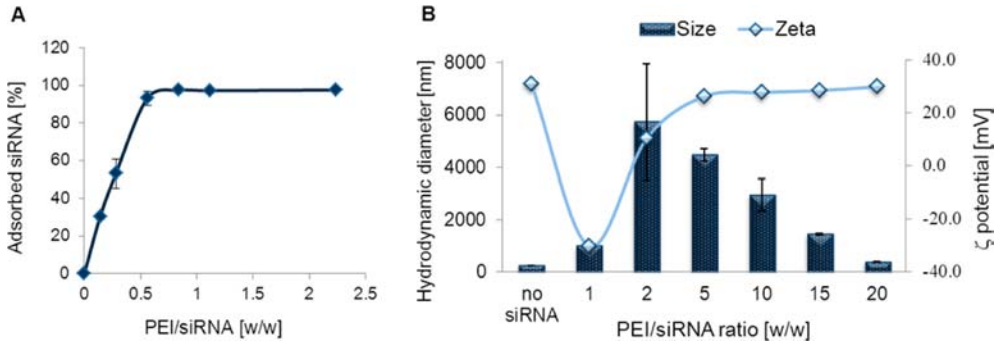

Figure 3. (A) Curve of siRNA adsorption onto SPEI NPs, (B) Size and ζ potential of SPEI/siRNA polyplexes in deionized H_2O. In both charts, the horizontal axes represent PEI/siRNA mass ratio.

the total PEI amount constituting SPEI NPs could be readily calculated by subtracting the weight loss contributions of the two final weight loss stages of SDVS NPs (12.67% w/w, Table 4) from the three final weight loss steps of functional SPEI NPs (18.16% w/w, Table 4) in corresponding TGA profiles. In this manner, the calculated weight amount for the PEI phase has been found to be close to 5.5% when excluding weight loss contributions from any adsorbed volatile solvent(s) and/or reagent(s).

Furthermore, comparison of differently PEI-modified SiO_2 NPs (covalent vs noncovalent attachment) demonstrates quite significant differences in both DTG and DSC profiles (Figure S4). These thermogravimetric data confirmed the relevance of this novel NP-binding DVS chemistry. More specifically, PEI-decorated NPs (noncovalent mode of PEI attachment) showed a quite smooth temperature-dependent wavy DSC profile that is much different from the linearly decreasing profile of SPEI NPs (covalent mode of PEI attachment). These data revealed the likely smoothing effect of the DVS-mediated covalent attachment of the multiweighted PEI polymeric phase in SPEI NPs (Figure S4-A). In addition, the weight loss step that mainly contributed to PEI thermal decomposition (354 °C DTG minimum, Figure S3-E) clearly shifted toward a lower temperature (280 vs 343 °C) and appeared less defined for PEI noncovalent binding mode NPs than that related to SPEI NPs (Figure S4–B).

Beyond the quantification aspect of NP characterization, FTIR spectroscopy (Figure S4) of the four starting (pure SiO_2 NPs) and differently modified SPA, SDVS, and SPEI NPs provided tracking of functionality in agreement with the designed fabrication of the corresponding NPs. For example, in all spectra, there are vibration bands arising from asymmetric vibrations of Si–O–Si (1109 and 810 cm^{-1}), Si–OH (966 cm^{-1}) bonds, as well as symmetric vibrations of Si–O–Si bonds (812 cm^{-1}).[44] Adsorbed and/or interstitial H_2O shows an intense characteristic absorption band between 3300 and 3500 cm^{-1} that is assigned to O–H stretching in H-bonded H_2O. This adsorption band is accompanied by a characteristic strong 1635 cm^{-1} band that is due to scissor-bending vibrations of molecular H_2O.[45] Moreover, absorption bands at 1520–1570 cm^{-1} are related to both primary and secondary amine N–H bends, while the band at 1456–1477 cm^{-1} can be readily assigned to methylene C–H bends.[46] Both area adsorptions significantly increased after PEI attachment, while they are not present in nondecorated SiO_2 NPs.

Polyplex Formation Ability of SPEI NPs with siRNA. The complexation ability of functional polycationic SPEI NPs with siRNA sequences was confirmed by UV absorption measurements (Nanodrop instrument) using ultrasmall microliter-sized volumes. In this manner, different amounts of SPEI NPs were incubated with the same concentration of siRNA (12.4 μM, 15 min, ambient temperature) and then centrifuged (13,000 rpm) to precipitate siRNA-NPs polyplexes. The concentration of unbound siRNA was then measured at 260 nm by comparison with a control sample that did not contain any NP. The corresponding complexation results are summarized and represented as percentages of bound siRNA as a function of PEI/siRNA w/w ratios (Figure 3A). At PEI/siRNA ratios lower than 0.56, the complexation is rather weak and clearly does not reach saturation. In contrast, at a PEI/siRNA ratio of 0.56, nearly all the negatively charged siRNA has bound to the positively charged SPEI NPs, with a 93% efficacy. At higher PEI/siRNA ratios, the siRNA release is relatively low, less than 2%, confirming its high affinity toward polycationic SPEI NPs.

During such SPEI NPs/siRNA polyplex formation, additional tracking of both physicochemical loaded NP hydrodynamic diameter (polyplex aggregation level) and ζ potential (NP surface charge) parameters has been performed to better characterize polyplex formation and behavior (Figure 3B). The

dx.doi.org/10.1021/bc4004316 | Bioconjugate Chem. 2013, 24, 2076–2087

corresponding samples were prepared using variably increasing w/w PEI/siRNA ratios, with a maximum value of 20 (Figure 3B). The samples were prepared by contacting a constant amount of SPEI NPs (200 μg) with variably decreasing amounts of siRNA in deionized H_2O (15 min incubation) and subsequently diluting with H_2O up to 1 mL to obtain constant (0.2 mg/mL) NP-concentration suspensions. As expected, bare unloaded SPEI NPs are highly positively charged (ζ potential: +31.1 mV), with an average hydrodynamic diameter of 258 nm. Following siRNA complexation, polyplex ζ potential values generally became negative/less positive, depending on the polyplex composition. In addition, the DLS average diameter of these same polyplexes also depended on its dual component combination, increasing with decreasing ζ potential absolute value (NP charge neutralization). For instance, at a PEI/siRNA ratio of 1:1, ζ potential is negative, reaching −30.1 mV and resulting in a mild aggregation phenomenon that affords 1011 nm polyplexes. Lower siRNA percentages (2−20 PEI/siRNA w/w ratios) afforded ζ potential values that became increasingly positive and approached the initial value (+31.1 mV) obtained when no siRNA was added. The average hydrodynamic size of the 2:1 PEI/siRNA w/w combination showed a clear tendency toward acute aggregation (5729 nm) and demonstrated a +10.4 mV ζ potential value. Recovery of the positive surface charge (+26.3, +27.8, and +28.5 mV) at 5:1, 10:1, and 15:1 PEI/siRNA w/w ratios, respectively, led to reduction of the hydrodynamic sizes of the polyplexes (4462, 2946, and 1466 nm, respectively). At a PEI/siRNA w/w ratio of 20:1, the amount of siRNA was so small that it hardly affected the initial ζ potential value (+30.0 vs +31.1 mV) and the initial size of the polyplexes (394 vs 258 nm). These results may contribute to better understanding of how these factors affect siRNA delivery and silencing potential features of our SPEI NPs.

Nanoparticulate Polyplex Behavior in DMEM. Due to the use of a protein-rich biological DMEM in cell incubation, polyplex aggregating behavior has been investigated by tracking NP aggregation features during cell incubation (Figure 4). For

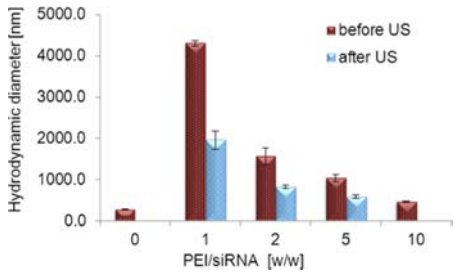

Figure 4. Hydrodynamic size of SPEI/siRNA polyplexes in DMEM before and after ultrasonic bath.

that purpose, hydrodynamic sizes of bare SPEI NPs and siRNA-loaded SPEI NPs/siRNA polyplexes at *four different weight ratios* were measured during 10 min NP incubation in a DMEM. In these experiments, a constant range of NP concentrations (0.2 mg/mL) has been used by incubating the SPEI NPs (120 μg) with variably decreasing siRNA amounts in deionized H_2O (≈60 μL, 15 min) and subsequently diluting with fresh DMEM (540 μL). In contrast to the DLS experiment, ζ potential could not be properly detected in this NP concentration range due to the relatively high ionic strength of the biological medium. The bare unloaded SPEI NPs showed good colloidal stability, with an average hydrodynamic diameter of 284 nm. The highest PEI/siRNA mass ratio used in silencing experiments (1:1) demonstrated the most aggregated behavior (≈4300 nm) of the polyplexes. Following reduction of the polyplex siRNA percentage, the colloidal stability of DMEM suspensions gradually recovered toward the initial state of the noncomplexed SPEI NPs, going through 1560 and 1037 to 467 nm for 2:1, 5:1, and 10:1 ratios, respectively. Resulting NP aggregates might be loosely bound, so the effect of a time-limited ultrasound (US) pulse (60 s US irradiation) has been tested for most aggregated samples. Figure 4 reports DLS diameters of NP aggregates measured *before* and *after* ultrasonication (ultrasonic bath) to investigate their degree of formation reversibility. These results proved that, in a DMEM, polyplex aggregation can be considered a reversible process for 1:1, 2:1, and 5:1 PEI/siRNA mass ratios. These data emphasized the interesting fact that the actual effective silencing agents are micrometer-sized, rather than nanosized, NP aggregates that likely fragmented during cell membrane contact and particle cellular internalization.

Chemical Stability of SPEI NPs − Storage Issue. During silencing studies, it has been observed that aqueous dispersions of SPEI NPs older than two weeks disclosed a much weaker silencing effect than fresh dispersions when tested in similar conditions (75% rather than current effective 90% gene silencing capability by 5:1 PEI/siRNA ratio, 100 nM siRNA). A likely reason for this unexpected phenomenon might be PEI 25 kDa detachment from the NP surface due to the hydrolysis of APTS-based covalent Si−O linkages. Interestingly, the current literature in the field has never reported such a result. In the case of SPEI NPs, this phenomenon has been readily quantified using a Kaiser Test for free NH_2 groups in supernatants collected from centrifuge-precipitated SPEI NPs and dispersed in both deionized H_2O and EtOH; the times of contact at 4 °C (fridge storage) were 7 weeks and 5.5 months, respectively. Kaiser Test values for hydrolyzed PEI species in supernatants were compared and calibrated with standard 0.1 μg/μL 25 kDa PEI EtOH and H_2O solutions (Table S1). The corresponding results indicated nearly complete detachment of more than 95% of PEI species occurred for the 7 week contact period as an aqueous dispersion. In contrast, only partial detachment of less than 20% has been measured for the 5 month storage of NPs in EtOH dispersion. Moreover, in this final case, EtOH storage of SPEI NPs at 4 °C strictly preserved the NP overall silencing effectiveness even after 1 year of EtOH cold storage. This time dependent confirmation of gene silencing capabilities of stored SPEI NPs in liquid suspensions has significance for the optimal use of this nanoscale delivery system for effective gene silencing.

Confocal Microscopy of the Cellular Uptake of SPEI NPs/siRNA Polyplexes. The cellular uptake of SPEI NPs/siRNA polyplexes was confirmed using fluorescent confocal microscopy (Figure 5). In this study, we used fluorescent FITC-labeled SPEI NPs and nonfluorescent siRNA species. For that purpose, core fluorescent 34.0 nm FITC-labeled SiO_2 NPs have been readily prepared using a known procedure [47] built on the base-catalyzed cohydrolysis of TEOS and of a fluorescent FITC-APTS conjugate (≈0.02 molar %; see the Materials and Methods for protocol details). This method resulted in the covalent incorporation of the FITC dye within a fabricated hybrid NP inorganic SiO_2 matrix. Such FITC-labeled hybrid SiO_2 NPs disclosed very similar size, size distribution, and ζ potential characteristics when compared to nonfluorescent NPs. During cellular uptake experiments, the colocalization of

dx.doi.org/10.1021/bc4004316 | *Bioconjugate Chem.* 2013, 24, 2076−2087

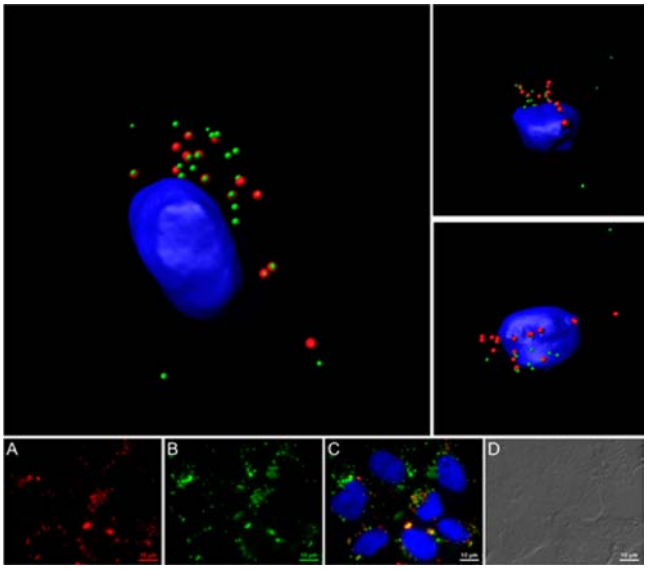

Figure 5. (*Top*) 3D images of a single U2OS cell incubated with FITC-labeled SPEI NPs/siRNA polyplexes. Both cell nucleus and lysosome compartment have been stained with DAPI and LysoTracker, respectively. (*Bottom*) 2D image of U2OS cells incubated with FITC-labeled SPEI NPs/siRNA polyplexes: (A) Lysosomes stained with LysoTracker (cy3 filter), (B) incubated FITC-labeled SPEI NPs/siRNA polyplexes (40/1 w/w preparation), (C) merged filtered image (lysosome and polyplexes), and (D) DIC image of the same U2OS cells.

hybrid SPEI NPs/siRNA polyplexes with the lysosome compartment has been evidenced by compartment staining with a LysoTracker reagent (red spot visualization). These red spots (Figure 5A) were generally found to colocalize with green spots arising from hybrid SPEI NPs (Figure 5B), producing color-mixed yellow and orange spots (Figure 5C). This fluorescence-based colocalization experiment indicated that the cell internalization of corresponding polyplexes arose via the endocytic pathway. The lysosome is the final and most acidic compartment of the cellular endocytic pathway where digestion of waste materials and foreign agents mainly takes place. A 3D fluorescence-based image of a single cell has also been generated using a set of 2D sectional subimages (*z* stacking) obtained by confocal microscopy (Imaris software, Figure 5 top). Interestingly, part of the visible green fluorescent spots did not colocalize with lysosomes. A possible explanation for such a phenomenon is that not all the NPs entered the lysosome and remained in the early and late endosomes surrounding the nucleus. As clearly shown by both 2D and 3D microphotographs, green fluorescence signals only appeared in the cell cytoplasm but not in the nuclear area, meaning that SPEI NPs/siRNA polyplexes could not penetrate the cell nucleus through its membrane. In conclusion, this observed effective cellular uptake of SPEI NPs/siRNA polyplexes, concomitant with a corresponding construct lysosome/endosome escape, are the key factors for cytoplasmic RNAi-mediated gene silencing.

SPEI NPs Efficiently Silence Gene by RNAi. To test the efficacy of previously fabricated polyplexes in induction of gene silencing, we used a well-known two-gene reporter system based on two luciferase proteins, 61 kDa *Firefly* and 36 kDa *Renilla*, in stably transfected dual-transporter U2OS cells. Luciferases belong to a class of oxidative enzymes that emit photons during the oxidation of a specific substrate to produce bioluminescence. The dual luciferase system enabled measuring the specific silencing (*Firefly*), whereas the *Renilla* remained unchanged unless the NP introduced toxicity, thus causing cell death and reduction in the enzyme level compared to control (cells untreated with NPs). Any toxicity caused by SPEI NP will reduce the activity of both genes. It is also worthwhile to notice that, although SPA NPs possess multiple surface NH_2-groups, they were not tested in our silencing system as their ability to deliver electrostatically bound polynucleotides was already evidenced to be quite limited.[48,49]

The down-regulation of the *Firefly* luciferase was conducted using a constant amount of siRNA (100 nM) that was loaded using different NP weights and resulted in six different (1.0–20.0) PEI/siRNA mass ratios (Figure 6A). In order to compare SPEI NPs arising from surface decoration using grafted 25 kDa PEI, i.e., covalently attached versus nonmodified, free PEI as siRNA delivery agent, we used common units of the polyplex ratio that characterized both PEI to siRNA weight contents instead of NP/siRNA weight ratios. All the described silencing results were collected using *one year-old* SPEI NPs that demonstrated a same silencing activity than the one observed with *freshly prepared* SPEI NPs. Gene activities were tested after a 48 h treatment using a Dual-Luciferase assay (Experimental Section). At a 1:1 weight ratio, there is already a high level of *Firefly* luciferase silencing (69%) along with high cellular viability. Furthermore, and as expected, higher 2:1 and 5:1 PEI/siRNA ratios exhibit even more pronounced silencing effects, 90% and 89%, respectively, without any observed cellular

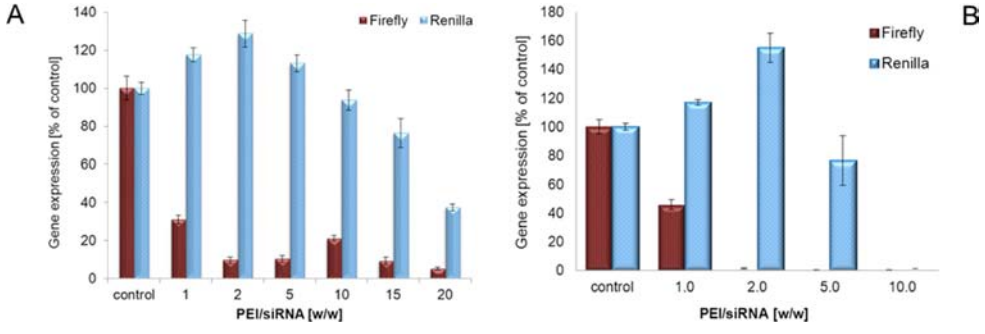

Figure 6. siRNA delivery to stably transfected dual-transporter U2OS cells. Luciferase expression levels were measured 48 h after transfection without any medium change and are presented here as % gene expression relative to untreated control cells. The horizontal axes represent the weight ratios of both PEI and siRNA components. The final siRNA concentration in each culture medium was maintained at 100 nM. Different (A) SPEI NPs/siRNA and (B) free 25 kDa PEI/siRNA mass ratio polyplexes were used to transfect *Firefly* luciferase-specific siRNA.

dx.doi.org/10.1021/bc4004316 | *Bioconjugate Chem.* 2013, 24, 2076–2087

toxicity. Further increased PEI/siRNA mass ratios disclosed clear cellular cytotoxic effects, with no improvement in gene silencing, which is likely caused by the high dosage of highly positively charged SPEI NPs/siRNA polyplexes (Figure 3B). These results emphasized the optimal 2:1−5:1 range of PEI/siRNA weight ratios for effective siRNA delivery and gene silencing. The lowest 1:1 PEI/siRNA ratio resulted in negatively charged polyplexes (−30.1 mV) that likely experienced increased difficulty to induce lysosome rupturing (the "proton sponge" effect), which is essential for NP escape into the cell cytosol where the silencing machinery exits.

Figure 6B describes silencing results observed for the nonmodified free 25 kDa PEI in a 1.0−10.0 PEI/siRNA weight ratio range. They clearly demonstrated a high silencing efficiency at a 2:1 ratio along with a high cytotoxicity for the 10:1 ratio, where *Renilla* expression stands at a zero level. Using common units for polyplex composition ratios enabled to compare both silencing systems of SPEI NPs and free 25 kDa PEI. Obviously, the same PEI content in SPEI NPs/siRNA polyplexes caused much less toxicity then free PEI, meaning with a 94% level *Renilla* expression versus a zero level one respectively.

To further improve the overall efficiency of such an effective nanosystem, lower concentrations of siRNA as gene silencing agent have also been tested. Figure 6B shows *Firefly* silencing when using variably decreasing siRNA molar concentrations for a constant 5:1 w/w PEI/siRNA mass ratio that previously proved to be effective (Figure 7). Interestingly, low (41%) to

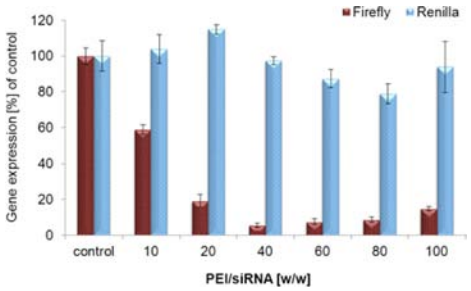

Figure 7. Different molar concentrations of *Firefly* luciferase-specific siRNA were used for transfection. The weight ratios of PEI/siRNA polyplexes were maintained at 5:1. The horizontal axis represents siRNA molar concentration.

quite significant (81 and 95%) levels of gene knockdown can already be observed for the lowest (10 nM) and slightly higher (20 and 40 nM) concentrations, respectively. At higher concentrations of siRNA (60, 80, and 100 nM), no improvement occurred. This result highlighted the effectiveness of the 5:1 PEI/siRNA particulate composition with a 40 nM total concentration of siRNA with no cytotoxicity.

DISCUSSION

In this study, we introduced a novel method of controlled covalent surface decoration and component assembly design for the effective fabrication of polycationic nanoscale carrier SiO_2 particles. The resulting functional SiO_2 NPs possess a covalently grafted 25 kDa branched PEI polymeric shell enabling both siRNA delivery and gene silencing. This key grafting step for both SiO_2 and PEI component assembly utilized an innovative and powerful C2 symmetric divinyl sulfone (DVS, $(CH_2{=}CH)_2SO_2$) *bis*-Michäel acceptor toward nucleophilic chemical species. This *covalent grafting* method has been characterized by its (i) overall efficacy for the controlled assembly of both inorganic SiO_2 and organic PEI phases, (ii) easy reproducible and efficient fabrication protocol, (iii) requirement of relatively simple and inexpensive reagents, and finally, (iv) efficient silencing via binding of siRNA.

In addition, all the corresponding NP surface modification steps that resulted in functional intermediate and final NPs have been fully characterized using a wide range of analytical, spectroscopic, and microscopy methods. From SPEI NPs/siRNA adsorption curves, we also learned that the formation of stable polyplexes took place at a PEI/siRNA mass ratio (0.56) lower than the one for optimal silencing induction (2.00). That result suggested that the PEI present on the NP acted not only for siRNA binding but also for the induction of the NP endosomal escape.

DLS measurements (NP hydrodynamic size) of the SPEI NPs/siRNA polyplexes in real cell incubation conditions (DMEM) showed relatively stable dispersion qualities and a moderate degree of aggregation. In addition, when using 60-s-long ultrasound pulses, this aggregation phenomenon has been demonstrated to be partially reversible. It suggested that DMEM-aggregated SPEI NPs might readily disaggregate during cell-SPEI NP interactions, thus rationalizing the observed efficient gene silencing.

Importantly and regarding SPEI NPs, we also conducted time-dependent thermodynamic stability tests. They disclosed that SPEI NP silencing capabilities may be preserved *for more than one year* when stored in cold EtOH. This property reflects the high chemical stability of the DVS-mediated covalent attachment of the PEI phase onto the NP surface. Such a feature was found only weakly affected during SPEI NPs storage in dehydrated conditions.

Furthermore, this siRNA nanoscale delivery agent, SPEI NPs, has been shown to readily assemble with the gene silencing machinery with no toxicity induction when using a PEI concentration lower than 16 μg/mL as present on around 300 μg/mL SPEI NP suspension. This last feature most likely arose from the covalent DVS-grafting of a quite thin layer of 25 kDa branched PEI polymer (5.5% weight) that was stably present on the NP outer shell. Indeed, the covalent binding of PEI reduced its toxicity compared to the same amount of free PEI due to its interactions with the silica carrier.[50] Another advantage of our siRNA delivery vehicle originates from the siRNA binding on the outer shell of SPEI NPs rather than being encapsulated within the nanomaterial matrix or pores. This strategy promotes high potency in siRNA release in cytosol as evidenced by the quite high level of gene silencing (95%). Moreover, the dual-luciferase-transfected cell system provided high throughput silencing results with very precise signal quantification ability while harboring a built-in internal control for cytotoxicity examination. In general, these SPEI NPs offer great opportunities for further functionalization by addition of targeting peptides (via their covalent binding to PEI), generating particles that can potentially silence while being specifically targeted to any desired site within the body.

CONCLUSIONS

A novel method for the covalent attachment of a 25 kDa PEI polymer onto poly-NH_2-SiO_2 NPs was achieved by divinyl sulfone (DVS)-mediated Michäel addition chemistry. Resulting optimal 34.2 ± 4.2 nm SPEI NPs possess a hydrodynamic diameter of 304.7 ± 4.9 nm, a ζ potential of 26.6 ± 1.0 mV, and a PEI (polycationic shell) weight percentage of 5.6%. SPEI NPs

dx.doi.org/10.1021/bc4004316 | *Bioconjugate Chem.* 2013, 24, 2076−2087

were found to effectively bind siRNAs to form corresponding polyplexes in aqueous media resulting in controlled changes in NP hydrodynamic sizes and ζ potentials. Tracking the hydrodynamic behavior of the polyplexes in DMEM pointed to a controllable aggregation phenomenon even in the presence of serum proteins. The polyplex cellular uptake was found mediated by the endocytic pathway resulting in polyplex endosomal entrapment. Its subsequent liberation occurred due to a clear SPEI NP/siRNA ability to induce the "proton sponge" effect. *In vitro* gene silencing was tested using a dual-luciferase (*Firefly*/*Renilla*) transgenic cell system where *Firefly* was the target gene for knockdown, whereas *Renilla* served as a control for cytotoxic effect traceability. An optimal SPEI NP formulation regarding both silencing and NP cytotoxicity level was set up by selecting specific factors that included an optimal SPEI NP/siRNA weight ratio and siRNA concentration resulting in a silencing degree of up to 95% compared to untreated cells. Moreover and quite importantly, this innovative DVS-mediated mode of covalent grafting of the polycationic PEI polymeric phase onto the surface of SPEI NPs has been shown to positively mitigate the overall cellular toxicity of corresponding NPs. In addition, as-fabricated SPEI NPs are also characterized by their NP surface chemical versatility for modifications. For example, further SPEI NP functionalization by covalent binding of targeting peptides using such a functional PEI corona will enable the generation of efficient nanoscale carriers for siRNA delivery along with specific targeting capability to cancer cells (diseased organ specificity).

■ ASSOCIATED CONTENT

Ⓢ Supporting Information

Dynamic light scattering (DLS), ζ potential, amine group quantification (Kaiser Test), TGA/DTG and DSC analyses, FTIR spectroscopy, SPEI NPs & shell chemical stability investigation. This material is available free of charge via the Internet at http://pubs.acs.org.

■ AUTHOR INFORMATION

Corresponding Authors

*Tel.: +972 3 531 8068; fax: +972 3 535 1824. E-mail address: michaes@mail.biu.ac.il.

*Tel.: +972 3 531 8324; fax: +972 3 738 4053. E-mail address: jean-paul.m.lellouche@biu.ac.il.

Author Contributions

Yekaterina Kapilov Buchman, Emmanuel Lellouche, and Sally Zigdon contributed equally to this work.

Notes

The authors declare no competing financial interest.

■ REFERENCES

(1) Bumcrot, D., Manoharan, M., Koteliansky, V., and Sah, D. W. Y. (2006) RNAi therapeutics: a potential new class of pharmaceutical drugs. *Nat. Chem. Biol. 2*, 711−719.

(2) Vaishnaw, A., Gollob, J., Gamba-Vitalo, C., Hutabarat, R., Sah, D., Meyers, R., de Fougerolles, T., and Maraganore, J. (2010) A status report on RNAi therapeutics. *Silence 1*, 14.

(3) Merdan, T., Kopeček, J., and Kissel, T. (2002) Prospects for cationic polymers in gene and oligonucleotide therapy against cancer. *Adv. Drug Delivery Rev. 54*, 715−758.

(4) Boyer, C., Teo, J., Phillips, P., Erlich, R. B., Sagnella, S., Sharbeen, G., Dwarte, T., Duong, H. T. T., Goldstein, D., Davis, T. P., Kavallaris, M., and McCarroll, J. (2013) Effective delivery of siRNA into cancer cells and tumors using well-defined biodegradable cationic star polymers. *Mol. Pharmaceutics 10*, 2435−2444.

(5) Cho, H. Y., Averick, S. E., Paredes, E., Wegner, K., Averick, A., Jurga, S., Das, S. R., and Matyjaszewski, K. (2013) Star polymers with a cationic core prepared by ATRP for cellular nucleic acids delivery. *Biomacromolecules 14*, 1262−1267.

(6) Nakase, I., Tanaka, G., and Futaki, S. (2013) Cell-penetrating peptides (CPPs) as a vector for the delivery of siRNAs into cells. *Mol. Biosyst. 9*, 855−861.

(7) van Asbeck, A. H., Beyerle, A., McNeill, H., Bovee-Geurts, P. H. M., Lindberg, S., Verdurmen, W. P. R., Hällbrink, M., Langel, Ü., Heidenreich, O., and Brock, R. (2013) Molecular Parameters of siRNA−cell penetrating peptide nanocomplexes for efficient cellular delivery. *ACS Nano 7*, 3797−3807.

(8) Schroeder, A., Levins, C. G., Cortez, C., Langer, R., and Anderson, D. G. (2010) Lipid-based nanotherapeutics for siRNA delivery. *J. Intern. Med. 267*, 9−21.

(9) Gomes-da-Silva, L. C., Fonseca, N. A., Moura, V., Pedroso de Lima, M. C., Simões, S., and Moreira, J. N. (2012) Lipid-based nanoparticles for siRNA delivery in cancer therapy: paradigms and challenges. *Acc. Chem. Res. 45*, 1163−1171.

(10) Godinho, B. M. D. C., Ogier, J. R., Darcy, R., Odriscoll, C. M., and Cryan, J. F. (2013) Self-assembling moified β-cyclodextrin nanoparticles as neuronal siRNA delivery vectors: focus on Huntington's disease. *Mol. Pharmaceutics 10*, 640−649.

(11) McCarthy, J., O'Neill, M. J., Bourre, L., Walsh, D., Quinlan, A., Hurley, G., Ogier, J., Shanahan, F., Melgar, S., Darcy, R., and O'Driscoll, C. M. (2013) Gene silencing of TNF-alpha in a murine model of acute colitis using a modified cyclodextrin delivery system. *J. Controlled Release 168*, 28−34.

(12) Biswas, S., Deshpande, P. P., Navarro, G., Dodwadkar, N. S., and Torchilin, V. P. (2013) Lipid modified triblock PAMAM-based nanocarriers for siRNA drug co-delivery. *Biomaterials 34*, 1289−1301.

(13) Liu, J., Gu, C., Cabigas, E. B., Pendergrass, K. D., Brown, M. E., Luo, Y., and Davis, M. E. (2013) Functionalized dendrimer-based delivery of angiotensin type 1 receptor siRNA for preserving cardiac function following infarction. *Biomaterials 34*, 3729−3736.

(14) Boyer, C., Priyanto, P., Davis, T. P., Pissuwan, D., Bulmus, V., Kavallaris, M., Teoh, W. Y., Amal, R., Carroll, M., Woodward, R., and St Pierre, T. (2010) Anti-fouling magnetic nanoparticles for siRNA delivery. *J. Mater. Chem. 20*, 255−265.

(15) Chen, C., Mei, H., Shi, W., Deng, J., Zhang, B., Guo, T., Wang, H., and Hu, Y. (2013) EGFP-EGF1-conjugated PLGA nanoparticles for targeted delivery of siRNA into injured brain microvascular endothelial cells for efficient RNA interference. *PLoS One 8*, e60860.

(16) Chen, C.-J., Wang, J.-C., Zhao, E.-Y., Gao, L.-Y., Feng, Q., Liu, X.-Y., Zhao, Z.-X., Ma, X.-F., Hou, W.-J., Zhang, L.-R., Lu, W.-L., and Zhang, Q. (2013) Self-assembly cationic nanoparticles based on cholesterol-grafted bioreducible poly(amidoamine) for siRNA delivery. *Biomaterials 34*, 5303−5316.

(17) Heinemann, D., Schomaker, M., Kalies, S., Schieck, M., Carlson, R., Escobar, H. M., Ripken, T., Meyer, H., and Heisterkamp, A. (2013) Gold nanoparticle mediated laser transfection for efficient siRNA mediated gene knock down. *PLoS One 8*, e58604.

(18) Jagani, H. V., Josyula, V. R., Palanimuthu, V. R., Hariharapura, R. C., and Gang, S. S. (2013) Improvement of therapeutic efficacy of PLGA nanoformulation of siRNA targeting anti-apoptotic Bcl-2 through chitosan coating. *Eur. J. Pharm. Sci. 48*, 611−618.

(19) Vicennati, P., Giuliano, A., Ortaggi, G., and Masotti, A. (2008) Polyethylenimine in medicinal chemistry. *Curr. Med. Chem. 15*, 2826−2839.

(20) Guenther, M., Lipka, J., Malek, A., Gutsch, D., Kreyling, W., and Aigner, A. (2011) Polyethylenimines for RNAi-mediated gene targeting in vivo and siRNA delivery to the lung. *Eur. J. Pharm. Biopharm. 77*, 438−449.

(21) Nimesh, S. (2012) Polyethylenimine as a promising vector for targeted siRNA delivery. *Curr. Clin. Pharmacol. 7*, 121−130.

(22) Aravindan, L., Bicknell, K. A., Brooks, G., Khutoryanskiy, V. V., and Williams, A. C.A comparison of thiolated and disulfide-crosslinked

polyethylenimine for nonviral gene delivery. *Macromol. Biosci.*2013; Epub ahead of print.
(23) Tian, H., Li, F., Chen, J., Huang, Y., and Chen, X. (2012) N-isopropylacrylamide-modified polyethylenimines as effective gene carriers. *Macromol. Biosci. 12*, 1680−1688.
(24) Cheng, W., Yang, C., Hedrick, J. L., Williams, D. F., Yang, Y. Y., and Ashton-Rickardt, P. G. (2013) Delivery of a granzyme B inhibitor gene using carbamate-mannose modified PEI protects against cytotoxic lymphocyte killing. *Biomaterials 34*, 3697−3705.
(25) Lo, Y.-L., Sung, K.-H., Chiu, C.-C., and Wang, L.-F. (2013) Chemically conjugating polyethylenimine with chondroitin sulfate to promote CD44-mediated endocytosis for gene delivery. *Mol. Pharmaceutics 10*, 664−676.
(26) Tripathi, S. K., Singh, V. P., Gupta, K. C., and Kumar, P. (2013) Hydrophobic and membrane permeable polyethylenimine nanoparticles efficiently deliver nucleic acids in vitro and in vivo. *J. Mater. Chem. B 1*, 2515−2524.
(27) Wen, S., Zheng, F., Shen, M., and Shi, X. (2013) Surface modification and PEGylation of branched polyethyleneimine for improved biocompatibility. *J. Appl. Polym. Sci. 128*, 3807−3813.
(28) Badruddoza, A. Z. M., Rahman, M. T., Ghosh, S., Hossain, M. Z., Shi, J., Hidajat, K., and Uddin, M. S. (2013) β-Cyclodextrin conjugated magnetic, fluorescent silica core-shell nanoparticles for biomedical applications. *Carbohydr. Polym. 95*, 449−457.
(29) Kong, L., Mume, E., Triani, G., and Smith, S. V. (2013) Optimizing radiolabeling amine-functionalized silica nanoparticles using SarAr-NCS for applications in imaging and radiotherapy. *Langmuir 29*, 5609−5616.
(30) Sharma, P., Bengtsson, N. E., Walter, G. A., Sohn, H.-B., Zhou, G., Iwakuma, N., Zeng, H., Grobmyer, S. R., Scott, E. W., and Moudgil, B. M. (2012) Gadolinium-doped silica nanoparticles encapsulating indocyanine green for near infrared and magnetic resonance imaging. *Small 8*, 2856−2868.
(31) Singh, A. K., Hahn, M. A., Gutwein, L. G., Rule, M. C., Knapik, J. A., Moudgil, B. M., Grobmyer, S. R., and Brown, S. C. (2012) Multi-dye theranostic nanoparticle platform for bioimaging and cancer therapy. *Int. J. Nanomed. 7*, 2739−2750.
(32) Zhang, X., Yang, P., Dai, Y., Ma, P. a., Li, X., Cheng, Z., Hou, Z., Kang, X., Li, C., and Lin, J. (2013) Multifunctional up-converting nanocomposites with smart polymer brushes gated mesopores for cell imaging and thermo/pHdual-responsive drug controlled release. *Adv. Funct. Mater. 23*, 4067−4078.
(33) Xia, T., Kovochich, M., Liong, M., Meng, H., Kabehie, S., George, S., Zink, J. I., and Nel, A. E. (2009) Polyethyleneimine coating enhances the cellular uptake of mesoporous silica nanoparticles and allows safe delivery of siRNA and DNA cnstructs. *ACS Nano 3*, 3273−3286.
(34) Li, X., Xie, Q. R., Zhang, J., Xia, W., and Gu, H. (2011) The packaging of siRNA within the mesoporous structure of silica nanoparticles. *Biomaterials 32*, 9546−9556.
(35) Davies, W. G., Hardisty, E. W., Nevell, T. P., and Peters, R. H. (1970) The addition of alcohols to vinyl sulphones and sulphonamides. *J. Chem. Soc. B Phys. Org.*, 998−1004.
(36) Davies, W. G., Hardisty, E. W., Nevell, T. P., and Peters, R. H. (1970) The addition of amines to vinyl sulphones and sulphonamides. *J. Chem. Soc. B Phys. Org. 0*, 1004−1007.
(37) Imai, Y., Asamidori, Y., Inoue, T., and Ueda, M. (1981) Synthesis of polysulfone-sulfides by polyadditions of dithiols to divinyl sulfones. *J. Polym. Sci., Part A: Polym. Chem. 19*, 583−590.
(38) Green-Sadan, T., Kuttner, Y., Lublin-Tennenbaum, T., Kinor, N., Boguslavsky, Y., Margel, S., and Yadid, G. (2005) Glial cell line-derived neurotrophic factor-conjugated nanoparticles suppress acquisition of cocaine self-administration in rats. *Exp. Neurol. 194*, 97−105.
(39) Ziv, O., Avtalion, R. R., and Margel, S. (2008) Immunogenicity of bioactive magnetic nanoparticles: Natural and acquired antibodies. *J. Biomed. Mater. Res. A 85A*, 1011−1021.
(40) Sarin, V. K., Kent, S. B. H., Tam, J. P., and Merrifield, R. B. (1981) Quantitative monitoring of solid-phase peptide synthesis by the ninhydrin reaction. *Anal. Biochem. 117*, 147−157.
(41) Ring, R. N., Tesoro, G. C., and Moore, D. R. (1967) Kinetics of the addition of alcohols to activated vinyl compounds. *J. Org. Chem. 32*, 1091−1094.
(42) Zhuravlev, L. T. (2000) The surface chemistry of amorphous silica. Zhuravlev model. *Colloids Surf., A 173*, 1−38.
(43) Abdollahi, M., and Rouhani, M. (2012) Hydrophilic polymer/fumed silica hybrid nanoparticles synthesized via surface-initiated redox polymerization. *J. Polym. Res. 19*, 1−10.
(44) Kumar, V., Misra, N., Paul, J., Bhardwaj, Y. K., Goel, N. K., Francis, S., Sarma, K. S. S., and Varshney, L. (2013) Organic/inorganic nanocomposite coating of bisphenol A diglycidyl ether diacrylate containing silica nanoparticles via electron beam curing process. *Prog. Org. Coat. 76*, 1119−1126.
(45) Guang-She, L., Li-Ping, L., Smith, R. L., Jr, and Inomata, H. (2001) Characterization of the dispersion process for $NiFe_2O_4$ nanocrystals in a silica matrix with infrared spectroscopy and electron paramagnetic resonance. *J. Mol. Struct. 560*, 87−93.
(46) Coates, J., (2000) Interpretation of Infrared Spectra, A Practical Approach. *Encyclopedia of Analytical Chemistry* (Meyers, R. A., Eds.) Vol. 2, Wiley Online Library, Chichester.
(47) Ha, S.-W., Camalier, C. E., Beck, G. R., Jr, and Lee, J.-K. (2009) New method to prepare very stable and biocompatible fluorescent silica nanoparticles. *Chem. Commun.*, 2881−2883.
(48) Comiskey, G. A., Malefyt, A. P., Walton, S. P., Chen, C., and Baker, G. L.Surface functionalized silica nanoparticles for active transfection of siRNA, *PMSE Prepr.*2012.
(49) Suwalski, A., Dabboue, H., Delalande, A., Bensamoun, S. F., Canon, F., Midoux, P., Saillant, G., Klatzmann, D., Salvetat, J.-P., and Pichon, C. (2010) Accelerated Achilles tendon healing by PDGF gene delivery with mesoporous silica nanoparticles. *Biomaterials. 31*, 5237−5245.
(50) Zintchenko, A., Philipp, A., Dehshahri, A., and Wagner, E. (2008) Simple modifications of branched PEI lead to highly efficient siRNA carriers with Low toxicity. *Bioconjugate Chem. 19*, 1448−1455.